Magnetic rotation in ^{112}In

C. Y. He (贺创业),[1,*] X. Q. Li (李雪琴),[1] L. H. Zhu (竺礼华),[2,3] X. G. Wu (吴晓光),[1] B. Qi (亓斌),[4] Y. Liu (刘颖),[1]
B. Pan (潘波),[1] G. S. Li (李广生),[1] L. H. Li (李立华),[1] Z. M. Wang (王治民),[1]
Z. Y. Li (李忠宇),[5] S. Y. Wang (王守宇),[4] Q. Xu (徐强),[6] J. G. Wang (王建国),[6]
H. B. Ding (丁怀博),[6] and J. Zhai (翟健)[7]

[1]*China Institute of Atomic Energy, Beijing 102413, China*
[2]*School of Physics and Nuclear Energy Engineering, Beihang University, Beijing 100191, China*
[3]*School of Science, Shenzhen University, Shenzhen 518060, China*
[4]*School of Space Science and Physics, Shandong University at Weihai, Weihai 264209, China*
[5]*School of Physics and SK Laboratory of Nuclear Physics and Technology, Peking University, Beijing 100871, China*
[6]*Department of Physics, Tsinghua University, Beijing 100084, China*
[7]*Department of Physics, Jilin University, Changchun 130023, China*
(Received 11 November 2010; revised manuscript received 12 January 2011; published 16 February 2011)

The high spin states of ^{112}In have been investigated with in-beam γ-ray spectroscopic methods using the ^{110}Pd(^{7}Li,$5n$)^{112}In reaction at a beam energy of 50 MeV. A level scheme with three band structures has been established and their configurations are discussed. The positive-parity dipole band has been assigned as a magnetic rotation band. Particle-rotor model calculations have also been performed to interpret the rotational structures in ^{112}In.

I. INTRODUCTION

Many properties of nuclear rotation can be easily understood as being a consequence of certain symmetries [1]. Among them, chiral doublet bands in triaxial nuclei and shears bands in weakly deformed nuclei are two novel phenomena that have attracted significant interest in recent years. These two kinds of bands have been well interpreted by Frauendorf using the framework of the titled axis cranking model (TAC) [1,2]. Nuclei in the $A \sim 110$ mass region have been studid recently in search of bands exhibiting properties characteristic of the shears mechanism and chirality. In shears bands, the level energies follow a regular $I(I + 1)$ rule that appears similar to rotational bands in well-deformed nuclei, despite the small deformation of these nuclei in the proximity of the $Z = 50$ spherical shell gap. Such bands are also called magnetic rotation bands because of a substantial component of the magnetic dipole moment rotating around the axis of total angular momentum. Evidence of this phenomenon has already been reported in neutron-deficient ^{108,109,110}Cd [3–5] and ^{108,110,111,113}In [6–8] nuclei, which have $\Delta I = 1$ bands based on high-Ω $g_{9/2}$ proton holes and low-Ω $h_{11/2}$, $g_{7/2}/d_{5/2}$ neutrons. In addition, chiral rotation has also been proposed to occur in this region based on the TAC model [9], and this has been confirmed by experimental studies, such as the reported results for chiral doublet bands in the odd-odd Rh [10,11] and Ag [12,13] isotopes on the basis of the $\pi g_{9/2} \otimes \nu h_{11/2}$ configuration. The In isotopes are situated at the intersection of the island of chirality and the region where shears bands are predicted to appear in the area of $A \sim 110$. In a previous publication, the high spin levels of ^{108,110}In [6] were extensively researched and magnetic rotation bands were

found in the level structures, but there was no evidence for chiral rotations because of their low triaxial deformation [14]. In this respect, ^{112}In could be an interesting case where both shears bands and chiral bands can coexist since it is predicted to have $\gamma \sim 30°$ [14]. Although some low spin levels of ^{112}In have been studied via the reactions ^{110}Pd(^{6}Li,$4n\gamma$) [15], ^{112}Cd($p,n\gamma$) [16], and ^{109}Ag($\alpha,n\gamma$) [16], information regarding its level structure is still very limited. In this paper, we report on the experimental investigation of high spin states in ^{112}In and discuss newly found bands.

II. EXPERIMENTAL DETAILS

High spin states in ^{112}In were populated through the ^{110}Pd(^{7}Li,$5n$) reaction. The target consisted of a 2.4 mg/cm^2 foil of ^{110}Pd (isotopically enriched to 97.2%) backed with a 0.4 mg/cm^2 natural gold backing. The ^{7}Li beam was delivered by the HI-13 tandem accelerator at the China Institute of Atomic Energy. To determine the optimum beam energy for producing ^{112}In, γ-ray excitation functions were measured at beam energies of 40, 42, 46, 48, and 50 MeV. The experimental excitation functions for some intense γ rays observed in this experiment are presented in Fig. 1, which shows that the intensities of the known 187 and 588 keV transitions in ^{112}In increase with beam energies. Since 50 MeV was near the upper limit of accelerating ^{7}Li ions in the HI-13 accelerator, the beam energy of 50 MeV was chosen for the γ-γ coincidence measurement. An array consisting of 12 Compton-suppressed HPGe detectors and two planar HPGe detectors was used to collect γ-γ coincidence data. The Ge detectors in the array were placed at 90°, ±37°, ±30°, and ±60° relative to the beam direction. Each detector had an energy resolution of about 2 keV for 1332.5 keV γ rays. Energy and efficiency calibrations of the detectors were performed using standard
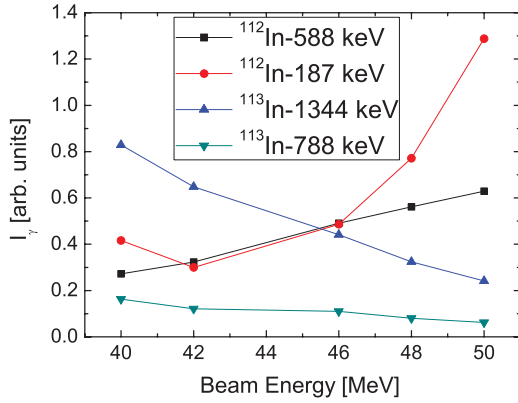
*chuangye.he@gmail.com

FIG. 1. (Color online) Excitation functions for the γ-ray transitions observed in the ^{110}Pd(^{7}Li,xn) reactions.

sources ^{60}Co and ^{152}Eu. In order to eliminate contamination from K-x rays of lead in the γ spectra, a lower threshold of 90 keV was set for these detectors. Events were collected, in event-by-event mode, when at least two Compton-suppressed Ge detectors fired in coincidence. A total of 200×10^6 γ-γ coincidence events were recorded. The data were sorted into a fully symmetrized E_γ-E_γ coincidence matrix, as well as into an asymmetric DCO (directional correlation ratios of oriented states) matrix. The DCO matrix was created by sorting the detectors at $\pm37°$ on one axis and the detectors at $\sim90°$ on the other. These matrices were analyzed with the RADWARE programs [17].

III. EXPERIMENTAL RESULTS

The excited states of ^{112}In have been studied previously by both Eibert *et al.* [15] and Kibédi *et al.* [16]. In these works, the low-spin transitions were identified and spins were pushed up respectively to $(10)\hbar$ and $8\hbar$ for the negative- and positive-parity bands. In the present work, many of the transitions from previous experiments are confirmed; in addition, the previous level is extended considerably with the placement of new transitions. Based on the γ-γ coincidence relations, together with the intensity balance of the transitions and the consistency of energy sums for the parallel decay paths with the DCO ratio analysis [18], the level scheme of ^{112}In is finally deduced, as presented in Fig. 2. It should be noted that Fig. 2 shows only a partial level scheme from our previous publication [19]. In the current paper, the discussion is focused on just bands 1–3. Figure 3 shows the plot of DCO ratios for most of the transitions included in the level scheme of ^{112}In, against γ transition energies. In our array geometry, if one gates on a dipole transition, the expected DCO ratios are close to 1.50 for stretched quadrupole transitions and around 1.0 for pure dipole transitions. The DCO values for the 187, 950, and 1413 keV transitions could not be determined because of low statistics for some weak γ rays or interference from contaminants. From the DCO ratios, the information from previous works [15,16], and systematic comparison with its neighboring odd-odd nucleus, we tentatively assigned the spins and parities of the levels in ^{112}In, as displayed in Fig. 2.
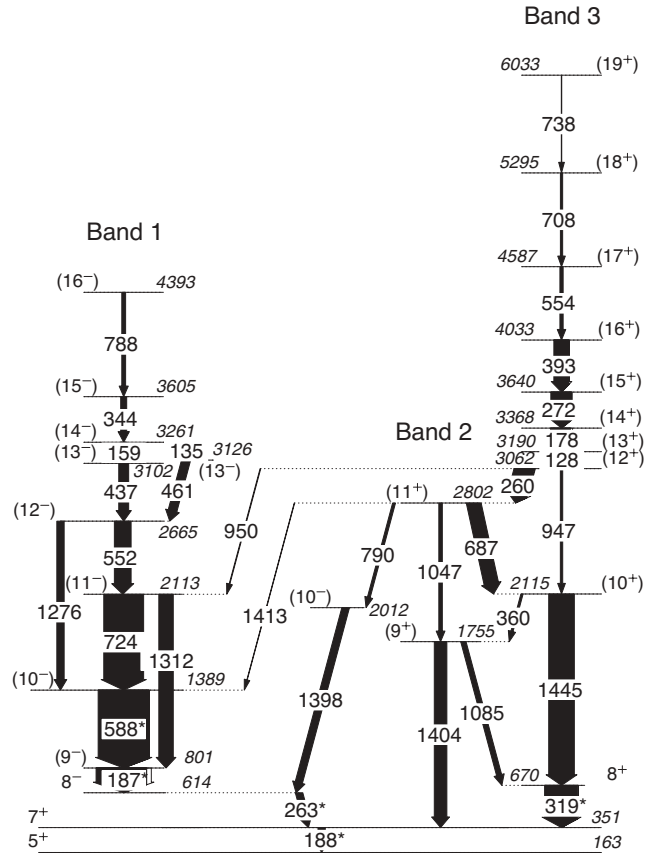

FIG. 2. Partial level scheme of ^{112}In obtained from the present experiment. It is built on the 5^+ state at 163 keV. The γ energies are in keV. The widths of the arrows are proportional to the intensities of the transitions. Transitions from the previous work are indicated by asterisks.

Table I shows the relative intensities and deduced DCO ratios for most of the γ transitions of ^{112}In in the present work.

The current study updates the ^{112}In level scheme greatly, including the addition of new bands (labeled 2 and 3 in Fig. 2) and the extension of the known sequence to higher spins. In the following we illustrate what has been extended or newly constructed in the level scheme: (A) band 1, whereby
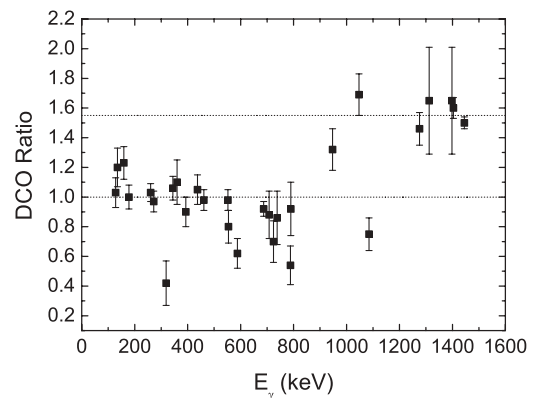

FIG. 3. DCO ratio vs γ-ray energies for most of the transitions in ^{112}In shown in Fig. 2.

TABLE I. γ-ray energies, relative γ-ray intensities, excitation energies, DCO ratios, multipolarities, and initial and final spin-parity assignments for each gamma ray in ^{112}In. The intensity for the 950 keV transition is not given here because of its low statistics.

E_γ (keV)	I_γ	E_i (keV)	R_{DCO}	Multi.	Assignment
187	134.7(5.0)	801			$(9^-)\rightarrow 8^-$
588	148.9(9.0)	1389	0.62(0.10)	$(M1)$	$(10^-)\rightarrow (9^-)$
1312	36.3(3.5)	2113	1.65(0.36)	$(E2)$	$(11^-)\rightarrow (9^-)$
724	100	2113	0.70(0.14)	$(M1)$	$(11^-)\rightarrow (10^-)$
1276	18.4(2.1)	2665	1.46(0.11)	$(E2)$	$(12^-)\rightarrow (10^-)$
552	40.5(6.4)	2665	0.98(0.07)	$(M1)$	$(12^-)\rightarrow (11^-)$
437	24.7(2.6)	3102	1.05(0.10)	$(M1)$	$(13^-)\rightarrow (12^-)$
461	22.1(2.4)	3126	0.98(0.07)	$(M1)$	$(13^-)\rightarrow (12^-)$
135	6.7(0.8)	3261	1.20(0.13)	$(M1)$	$(14^-)\rightarrow (13^-)$
159	13.6(1.2)	3261	1.23(0.11)	$(M1)$	$(14^-)\rightarrow (13^-)$
344	14.7(1.0)	3605	1.06(0.08)	$(M1)$	$(15^-)\rightarrow (14^-)$
788	9.56(0.8)	4393	0.54(0.13)	$(M1)$	$(16^-)\rightarrow (15^-)$
1398	18.6(2.6)	2012	1.65(0.36)	$(E2)$	$(10^-)\rightarrow 8^-$
790	7.0(0.5)	2802	0.92(0.18)	$(E1)$	$(11^+)\rightarrow (10^-)$
1413	1.6(0.2)	2802			$(11^+)\rightarrow (10^-)$
950		3062			$(12^+)\rightarrow (11^-)$
319	83.4(6.4)	670	0.42(0.15)	$M1$	$(8^+)\rightarrow 7^+$
1404	31.6(3.4)	1755	1.60(0.07)	$(E2)$	$(9^+)\rightarrow 7^+$
1445	64.6(3.7)	2115	1.50(0.04)	$(E2)$	$(10^+)\rightarrow 8^+$
1085	13.0(1.0)	1755	0.75(0.11)	$(M1)$	$(9^+)\rightarrow 8^+$
1047	8.8(0.7)	2802	1.69(0.14)	$(E2)$	$(11^+)\rightarrow (9^+)$
360	5.3(0.4)	2115	1.10(0.15)	$(M1)$	$(10^+)\rightarrow (9^+)$
947	5.9(0.4)	3062	1.32(0.14)	$(E2)$	$(12^+)\rightarrow (10^+)$
687	36.5(1.4)	2802	0.92(0.05)	$(M1)$	$(11^+)\rightarrow (10^+)$
260	50.0(2.4)	3062	1.03(0.06)	$(M1)$	$(12^+)\rightarrow (11^+)$
128	51.3(3.1)	3190	1.03(0.10)	$(M1)$	$(13^+)\rightarrow (12^+)$
178	50.1(1.9)	3368	1.00(0.08)	$(M1)$	$(14^+)\rightarrow (13^+)$
272	52.0(1.9)	3640	0.97(0.07)	$(M1)$	$(15^+)\rightarrow (14^+)$
393	38.0(4.6)	4033	0.90(0.10)	$(M1)$	$(16^+)\rightarrow (15^+)$
554	8.0(0.4)	4587	0.80(0.11)	$(M1)$	$(17^+)\rightarrow (16^+)$
708	9.5(0.1)	5295	0.88(0.16)	$(M1)$	$(18^+)\rightarrow (17^+)$
738	1.0(0.2)	6033	0.86(0.18)	$(M1)$	$(19^+)\rightarrow (18^+)$

the band is extended at higher energy with the new transitions of 724, 552, 437, 159, 344, and 788 keV, and the crossover $E2$ transitions with energies of 1312 and 1276 keV are also observed; some other transitions connecting band 1 to bands 2 and 3 are found with energies of 790, 1398, 1413, and 950 keV; (B) band 2, whereby the transitions are all observed for the first time, apart from the 319 keV transition from Ref. [17]; (C) band 3, which is a completely new band in the present work; it is built on the (12^+) state. As an example, Fig. 4 shows the representative coincidence γ-ray spectra by gating on the 461 keV (a), 1312 keV (b), 260 keV (c), and 128 keV (d) γ transitions, where the stronger coincidence peaks in bands 1, 2, and 3 can be seen.

IV. DISCUSSION

The yrast states in band 1 of the odd-odd ^{112}In are built on the 8^- state located at 614 keV above the 1^+ ground state [16]. Its configuration was assigned to $\pi g_{9/2}^{-1}\otimes\nu h_{11/2}$ in the previous work. For the situation in ^{112}In, the proton

Fermi level is located in the high-Ω orbital of the $\pi g_{9/2}$ subshell, while the neutron Fermi level lies at the bottom of the $\nu h_{11/2}$ subshell. Therefore, the perpendicular coupling of the angular momenta of the deformation-aligned proton and rotation-aligned neutron leads to a large magnetic moment with the band, thus manifesting as a magnetic dipole band. In the previous work, band 1 was only observed to $(10\hbar)$; it is extended to $(16\hbar)$ and a backbend is found in the present experiment. The observed spins I in band 1 are presented in Fig. 5 as functions of the rotational frequency ω, which for dipole bands is defined as $\hbar\omega(I) = E(I) - E(I-1)$. For comparison, $I(\omega)$ for a similar band in its adjacent isotope ^{110}In [6] is also plotted in Fig. 5. It is clear from Fig. 5 that both bands show very similar behaviors, including the frequencies of the alignments and the corresponding gains in spin. This suggests that the large backbend in ^{110}In is due to to the alignment of the first pair of positive-parity $g_{7/2}/d_{5/2}$ neutrons [6]. Band 1 in ^{112}In has, therefore, been assigned to $\pi g_{9/2}^{-1} \otimes \nu[h_{11/2}(g_{7/2}/d_{5/2})^2]$ after the backbend based on the $\pi g_{9/2}^{-1} \otimes \nu h_{11/2}$ configuration at low spins.

Band 2 is a new band deduced from the present experiment. The levels are connected by $E2$ transitions as well as by intermediate $M1$ transitions; the irregular sequence of these states suggests that it is not a good rotational structure because of its small deformation [20]. The level energy difference $E(I) - E(I-1)$ for these sets of levels obviously exhibits a signature (α) splitting when we analyze the γ transition energies. The splitting maybe results from the negative-γ deformation shape-driving effect of the high-Ω $g_{9/2}$ orbital. The energy differences for even I values are lower $(\alpha = 0)$ compared to the odd I $(\alpha = 1)$ values. Considering the Fermi surface for both protons and neutrons and the β deformation ~ 0.099 [20] of the low spin state of ^{112}In, it is evident that only the $g_{9/2}$ Nilsson orbital lies near the Fermi surface for the proton, while near the neutron Fermi surface the Nilsson orbitals are generally mixed in this mass region including the $g_{7/2}$ and $d_{5/2}$ orbitals. The neutron configuration of band 2 is probably coming from the $g_{7/2}$ or $d_{5/2}$ orbital, given the positive parity. Furthermore, the favored signature is defined as $\alpha_f = \frac{1}{2}[(-1)^{j_p-1/2} + (-1)^{j_n-1/2}]$ [21] for the odd-odd nucleus and it is clear that for ^{112}In, $j_p = 9/2$; thus j_n can only be specified as $7/2$ to satisfy the $\alpha = 0$ signature to be favored. Hence the configuration for band 2 is assigned to $\pi g_{9/2}^{-1} \otimes \nu g_{7/2}$.

The crossover transitions 1445 and 947 keV built on the known 8^+ state [16] in band 2 favor a positive parity for the spin with the $(12\hbar)$ state. Furthermore, the measured transitions in band 3 are tentatively assigned to the $M1$ multipolarity based on the DCO analysis; therefore the newly observed band 3 is very possibly a positive-parity band. It is built on the (12^+) state with an energy of 3062 keV, which is much higher than the energy of a two-quasiparticle bandhead. This may suggest that this is a four-quasiparticle band. The observed strong $M1$ transitions [see the spectrum gated by the 260 and 128 keV transitions in Figs. 4(c) and 4(d)] and lack of $E2$ crossover transitions denote a large magnetic moment for this band. Considering the proton and neutron numbers in ^{112}In, the configuration of band 3 is probably partially coming
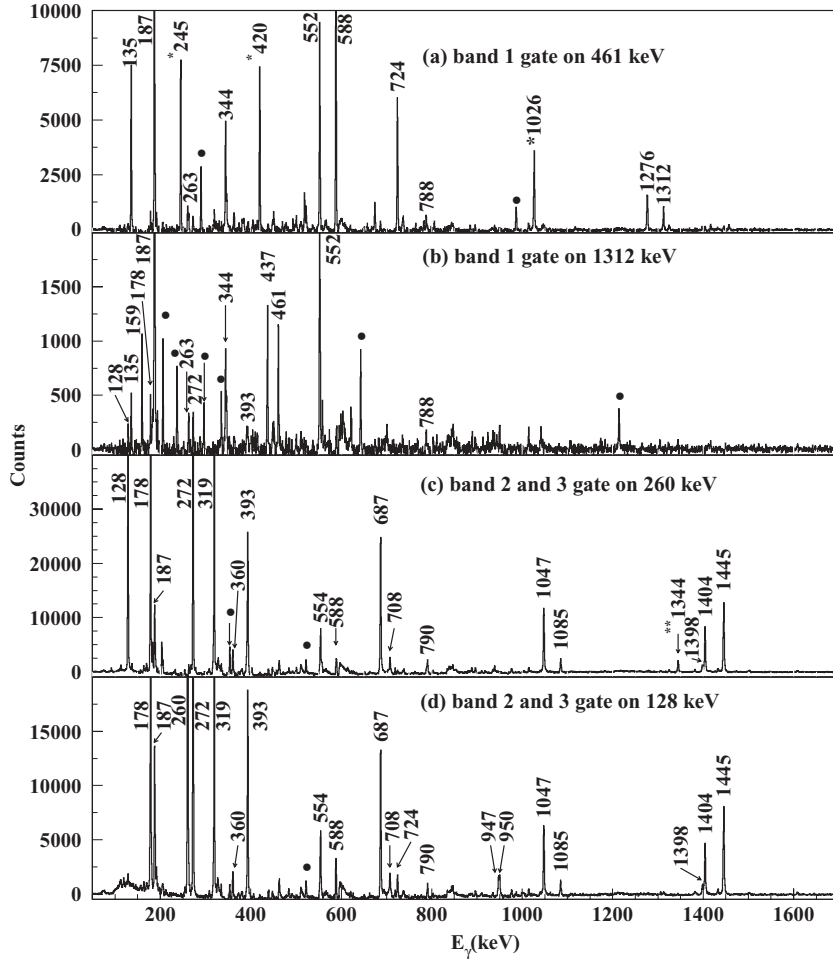
FIG. 4. Coincidence spectra obtained by (a) gating on 461 keV, (b) gating on 1312 keV, (c) gating on 260 keV, and (d) gating on 128 keV in ^{112}In. The peaks indicated with filled circles are associated with ^{112}In as reported in our previous publication [19]. The energies with single or double asterisks are contaminants from the reaction channels ^{197}Au(^{7}Li,4n)^{200}Pb or ^{110}Pd(^{7}Li,4n)^{113}In, respectively.

from the valence protons occupying the upper substates of the $g_{9/2}$ orbital and from the valence neutrons lying in the lower substates of the $h_{11/2}$ orbital. Moreover, the spin as a function of rotational frequency for band 3 plotted in Fig. 6 is very similar to that of band 3 in ^{110}In [6] up to 0.6 MeV. The band in ^{110}In has been reported with the configuration of $\pi g_{9/2}^{-1} \otimes \nu[h_{11/2}^{2}(g_{7/2}/d_{5/2})]$. Therefore, band 3 in ^{112}In may have a configuration similar to that of band 3 in ^{110}In. Since band 3 decays only into band 2 and the latter is assigned to $\pi g_{9/2}^{-1} \otimes \nu g_{7/2}$, the configuration for band 3 could be assigned to $\pi g_{9/2}^{-1} \otimes \nu(h_{11/2}^{2} g_{7/2})$.

Band 3 in ^{112}In can be understood as a result of the symmetry breaking related to the orientation of the angular momentum vector with respect to the nuclear shape, since the similar band in ^{110}In [6] has been assigned as a magnetic rotation band. The lack of $E2$ crossover transitions in band 3 indicates that this band is built on a weakly deformed structure. To interpret its structure, we have performed particle plus rotor model (PRM) calculations [22] for band 3 together with band 2 on the basis of the proposed configuration in the present work. In the calculations, the quadrupole deformation $\beta = 0.1$, $\gamma = 25°$, the empirical intrinsic quadrupole moment $Q_0 = 2.0$ eb, and gyromagnetic ratios $g_R = Z/A = 0.44$, $g_n(h_{11/2}) = -0.21$, $g_n(g_{7/2}) = 0.26$, and $g_p(g_{9/2}) = 1.26$ have been adopted. Figure 7 shows that the calculations well

reproduce the energy levels for both bands 2 and 3. This gives us more confidence on the configuration assignment for both bands 2 and 3. Band 3 is a magnetic dipole band, while band 2 is an electric quadrupole band. This indicates that they have structures that are dissimilar in nature. In order to better understand their rotational mode, $B(M1)/B(E2)$ ratios have also been calculated for them experimentally. Unfortunately, crossover $E2$ transitions were not discovered for band 3 in the
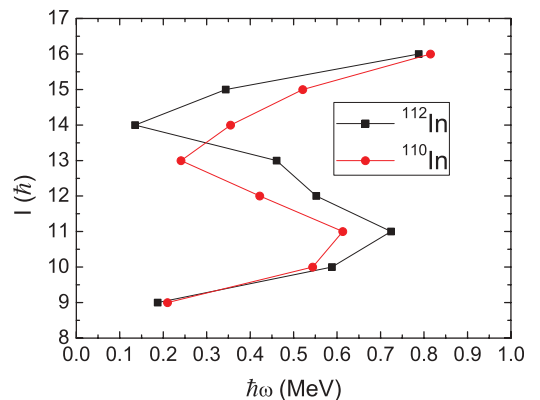

FIG. 5. (Color online) Angular momentum as a function of rotational frequency for band 1 in ^{112}In and bands 1 and 2 in ^{110}In [6].
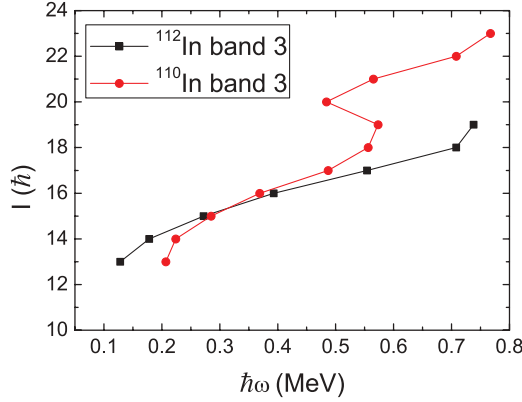
FIG. 6. (Color online) Angular momentum as a function of rotational frequency for band 3 in ^{112}In and band 3 in ^{110}In [6].

FIG. 8. (Color online) Experimental $B(M1)/B(E2)$ vs spin for band 2 and theoretical prediction of $B(M1)/B(E2)$ vs spin for both bands 2 and 3 in ^{112}In using PRM.

present experiment; we cannot compare the experimental data with the PRM calculations. Figure 8 shows much difference between the calculations and the experimental data for band 2. The PRM predicts that the $B(M1)/B(E2)$ ratios of band 2 remain nearly stable at lower spins and wobble at higher spins. However, the experimental values exhibit a rapid increase with spin, finally reaching the predicted value for band 3. The difference between the experimental results and the PRM calculations may be attributed to the rotation mode changing from collective to the shears mechanism with increasing spin. A similar phenomenon has been observed in the neighboring nucleus ^{109}Ag [23]. There, it was interpreted as an abrupt changing of the rotation axis. The situation is different in ^{112}In, however, in that the change in rotation axis may be occurring slowly with spin. The calculated $B(M1)/B(E2)$ ratios for band 3 in Fig. 8 have much higher values than those of band 2, and the values tend to go down with increasing spin, which is characteristic of the shears mechanism.

Both the experimental data and the PRM calculations discussed earlier exhibit characteristics of magnetic rotation for band 3. As reported in Ref. [24], the shears mechanism could be generated by the residual interaction between the proton and the neutron blades with a strength proportional to $P_2(\cos\theta)$, where θ is the shears angle. Experimentally, the
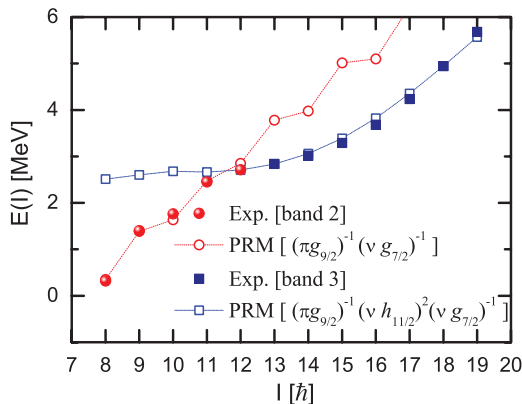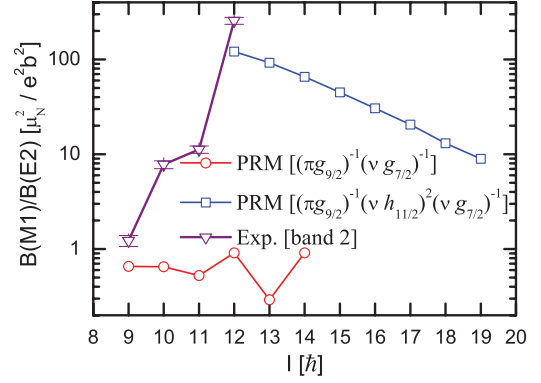

FIG. 7. (Color online) Experimental and theoretical prediction of $E(I)$ vs spin for bands 2 and 3 in ^{112}In using PRM.

shears angle for a pure shears band can be estimated at each observed spin I by calculating $\theta = \cos^{-1}[(I^2 - j_\pi^2 - j_\nu^2)/2 j_\pi j_\nu]$.

In real nuclei with small deformation, the excitation energy for each state usually comprises some collective contribution from the core; however, this portion has usually been neglected in previous studies [4,5]. Here, we assume the total spin to be $I = I_{\text{shears}} + R_{\text{core}}$, using a linear relation

$$R_{\text{core}}(I) = \frac{(\Delta R - R_{\text{core-bh}})I}{I_{\max} - I_{\text{bh}}} + \frac{I_{\max} R_{\text{core-bh}} - \Delta R I_{\text{bh}}}{I_{\max} - I_{\text{bh}}}, \quad (1)$$

where I_{bh} and $R_{\text{core-bh}}$ are the spin of the bandhead and angular momentum coming from core rotation at the bandhead. ΔR is determined from the difference between the maximum observed spin $I_{\max}$ and the sum of j_π and j_ν.

From the level energies and the angle θ between the proton and neutron spin blades, it is possible to obtain the effective interaction experimentally:

$$V_{\text{ex}}[I(\theta)] = E[I(\theta)] - E_{\text{bh}}, \quad (2)$$

where $V_{\text{ex}}[I(\theta)]$, $E[I(\theta)]$, and E_{bh} are the experimental value for the interactions coming from the shears mechanism, the energy of each level, and the bandhead energy, respectively. Since the shears angle is nearly 90° at the bandhead, E_{bh} could also be written as $E[I(90°)]$. Considering the small deformation of this nucleus, therefore, the energy contributed from the collective core in each level should be subtracted. Seeing that the level energy E in a well-deformed nucleus is usually assumed proportional to $I(I + 1)$, the energy contributed from the core is hereby supposed to be increasing in the same way:

$$E_{\text{core}}[I(\theta)] \approx E[I(\theta)] \frac{R_{\text{core}}^2(I)}{[I(\theta)]^2}. \quad (3)$$

The effective interaction between valence nucleons is finally deduced, $V[I(\theta)] = V_{\text{ex}}[I(\theta)] - V_{\text{core}}[I(\theta)]$, where $V_{\text{core}}[I(\theta)]$, which is defined similarly to $V_{\text{ex}}[I(\theta)]$, is the effective interaction coming from the collective core. Thus,

$$V[I(\theta)] = \{E[I(\theta)] - E_{\text{core}}[I(\theta)]\}$$
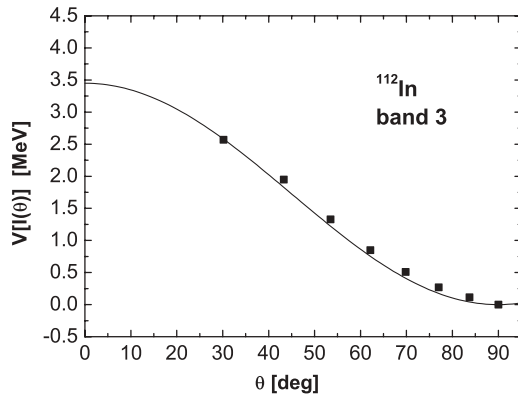$$- \{E[I(90°)] - E_{\text{core}}[I(90°)]\}. \quad (4)$$

FIG. 9. The effective interaction between valence protons and neutrons vs θ. The square dots show the experimental value for ^{112}In and the solid curve shows the theoretical calculation result.

On the other hand, the theoretical effective interaction between the valence protons and neutrons without collective contribution can be expanded in terms of even Legendre polynomials [25–27]; thus the relative energies of the interactions between valence particles could be expressed in a theoretical way:

$$V_{\text{th}}[I(\theta)] - V_{\text{th}}[I(90°)] = \frac{3V_2\cos^2\theta}{2}. \tag{5}$$

The strength of the effective interaction is determined here by the value of V_2 [28]. We calculated the energies of the states in band 3 relative to the $I = 12$ level by using the $\pi g_{9/2}^{-1}\otimes\nu(h_{11/2}^2 g_{7/2})$ configuration. The highest experimentally observed spin for this sequence is $I = 19$. The energies $V[I(\theta)]$ are plotted as a function of θ in Fig. 9. One can see in the figure that the values extracted from the experiment fit very well with the theoretical prediction. Taking into account one proton hole and three neutron particles as two blades of a pair of shears for band 3 in ^{112}In, we estimated that the interaction strength per proton-neutron pair is about 0.77 MeV, which is close to the values of 0.70 MeV and 0.75 MeV for

^{108,110}In, respectively. This provides further evidence that the interactions between these valence particles have a common origin in the shears mechanism.

As mentioned earlier in this paper, another main purpose of the present investigation is to search for chiral bands in ^{112}In. Chirality, however, has unfortunately not been discovered. Among the major qualifications for chiral bands, considerable collectivity is required; the rotational component R should be comparable in size to the proton and neutron spin vectors. Considering that the β deformation for the ground state of ^{112}In is only 0.099 [20], the contribution from the core is too limited to lead to the chiral symmetry being broken. Maybe this is the reason that we did not find chiral doublet bands in ^{112}In.

V. SUMMARY

In this work a detailed level scheme for the ^{112}In nucleus has been built from γ-ray spectroscopy study. Three band structures with 27 new γ transitions have been identified as belonging to ^{112}In. The backbend associated with the alignment of a pair of $g_{7/2}/d_{5/2}$ neutrons has been found in the negative-parity yrast band. The configuration for the positive parity yrare band has been assigned to $\pi g_{9/2}^{-1}\otimes\nu g_{7/2}$ for the lower spin states and $\pi g_{9/2}^{-1}\otimes\nu h^2{}_{11/2}(g_{7/2})$ for the higher spin levels. In addition, PRM calculations have also been employed for analysis of the nuclear structure of ^{112}In.

[1] S. Frauendorf, Rev. Mod. Phys. **73**, 463 (2001).

[2] S. Frauendorf and J. Meng, Nucl. Phys. A **617**, 131 (1997).

[3] N. S. Kelsall *et al.*, Phys. Rev. C **61**, 011301(R) (1999).

[4] C. J. Chiara *et al.*, Phys. Rev. C **61**, 034318 (2000).

[5] R. M. Clark *et al.*, Phys. Rev. Lett. **82**, 3220 (1999).

[6] C. J. Chiara *et al.*, Phys. Rev. C **64**, 054314 (2001).

[7] P. Vaska *et al.*, Phys. Rev. C **57**, 1634 (1998).

[8] S. Naguleswaran *et al.*, Phys. Rev. C **72**, 044304 (2005).

[9] J. Peng, J. Meng, and S. Q. Zhang, Phys. Rev. C **68**, 044324 (2003).

[10] C. Vaman, D. B. Fossan, T. Koike, K. Starosta, I. Y. Lee, and A. O. Macchiavelli, Phys. Rev. Lett. **92**, 032501 (2004).

[11] P. Joshi *et al.*, Phys. Lett. B **595**, 135 (2004).

[12] C. Y. He *et al.*, High Energy Phys. Nucl. Phys. **30(II)**, 166 (2006) (in Chinese).

[13] P. Joshi, M. P. Carpenter, D. B. Fossan, T. Koike, E. S. Paul, G. Rainovski, K. Starosta, C. Vaman, and R. Wadsworth, Phys. Rev. Lett. **98**, 102501 (2007).

[14] J. Meng, J. Peng, S. Q. Zhang, and S. G. Zhou, Phys. Rev. C **73**, 037303 (2006).

[15] M. Eibert, A. K. Gaigalas, and N. I. Greenberg, J. Phys. G **2**, L203 (1976).

[16] T. Kibédi, Zs. Dombrádi, T. Fényes, A. Krasznahorkay, J. Timár, Z. Gácsi, A. Passoja, V. Paar, and D. Vretenar, Phys. Rev. C **37**, 2391 (1988).

[17] D. C. Radford, Nucl. Instrum. Methods Phys. Res. A **361**, 297 (1995).

[18] G. S. Li, Chin. Phys. Lett. **16**, 796 (1999).

[19] C. Y. He *et al.*, Nucl. Phys. A **834**, 84c (2010).

[20] P. Möller, J. R. Nix, W. D. Myers, and W. J. Swiatecki, At. Data Nucl. Data Tables **59**, 185 (1995).

[21] I. Hamamoto, Phys. Lett. B **235**, 221 (1990).

[22] B. Qi, S. Q. Zhang, J. Menga, S. Y. Wangf, and S. Frauendorf, Phys. Lett. B **675**, 175 (2009).

[23] P. Datta *et al.*, Phys. Rev. C **78**, 021306(R) (2008).

[24] A. O. Macchiavelli, R. M. Clark, P. Fallon, M. A. Deleplanque, R. M. Diamond, R. Krücken, I. Y. Lee, F. S. Stephens, S. Asztalos, and K. Vetter, Phys. Rev. C **57**, 1073(R) (1998).

[25] J. P. Schiffer and W. W. True, Rev. Mod. Phys. **48**, 191 (1976).

[26] N. Anantaraman and J. P. Schiffer, Phys. Lett. B **37**, 229 (1971).

[27] A. Molinari, M. B. Johnson, H. A. Bethe, and W. M. Alberico, Nucl. Phys. A **239**, 45 (1975).

[28] R. M. Clark and A. O. Macchiavelli, Annu. Rev. Nucl. Part. Sci. **50**, 1 (2000).